The electronic contribution to metastability in age-hardening Al-Li alloys: a soft x-ray emission study

1995 J. Phys.: Condens. Matter 7 5405

(http://iopscience.iop.org/0953-8984/7/27/025)

J. Phys.: Condens. Matter 7 (1995) 5405–5416. Printed in the UK

The electronic contribution to metastability in age-hardening Al–Li alloys: a soft x-ray emission study

A Kerr†, L M Watson† and A Szasz‡

† Department of Metallurgy and Engineering Materials, University of Strathclyde, Colville Building, 48 North Portland Street, Glasgow G1 1XN, UK

‡ Department of Atomic Physics, Eotvos University, Muzeum krt. 6-8, H-1088 Budapest, Hungary

Received 13 March 1995

Abstract. A commercial 2091 aluminium–lithium alloy was subjected to various aging treatments to produce different metastable precipitates. The nature of the precipitates was deduced from differential thermal analysis and by reference to the literature. The Al $L_{2,3}$ and the Li Kβ spectra were recorded. The average energy of the Al $L_{2,3}$ emission band from the matrix was taken to be a measure of the overall energy of the valence electrons, and a direct correlation was established between the valence electron energy and the hardness of the alloy. The Li Kβ spectra from lithium concentrated in the precipitates showed considerable structure not present in the spectrum from the pure metal, and which is related to covalency in the Al–Li bonds.

1. Introduction

In many important alloy systems, physical properties can be altered by quenching from a high-temperature solid–solution field across a solvus line and aging at a temperature in the two-phase region of the equilibrium phase diagram. During aging, a number of metastable precipitates can be formed, which may be coherent or semi-coherent with the parent lattice, before the equilibrium phase appears. The lattice strain associated with these metastable precipitates is responsible for the strengthening of the alloy and much use is made of these mechanisms in commercial alloys. Although the strain energy of the lattice is increased, the metastability is associated with a local minimum in the free energy of the system, and the cause of this minimum is not well understood [1].

An important alloy system in this category which has received much attention over recent years because of its weight-saving potential in the aerospace industry, is the dilute lithium Al–Li system. The alloy studied in this work was the commercial aluminium alloy 2091 with a nominal composition of (wt%) 2.1 Cu, 2.0 Li, 1.5 Mg and 0.1 Zr. According to Sanders and Stark [2], a number of metastable precipitates can form from a supersaturated solid solution of this alloy, depending on aging temperature and time. These are listed in table 1.

This paper reports studies of the electronic structure of this alloy subjected to different aging treatments to produce different metastable states.

0953-8984/95/275405+12$19.50

Table 1.

Precipitate	Structure	Comment
δ'	Based on Al_3Li	Coherent with the α lattice
Θ'	Tetragonal based on Al_2Cu	Semicoherent, unlikely to form on prolonged aging with Mg present
S'	Orthorhombic based on Al_2CuMg	Semicoherent, main Cu bearing precipitate
T_1	Hexagonal based on Al_2MgLi	Equilibrium, likely to be suppressed in this alloy by formation of S'
T_2	Icosahedral based on Al_3CuLi_3	Stable between 170 and 520 °C

2. Experimental details

Soft x-ray emission spectroscopy was used to study the electronic structure of the alloys. The spectra give a measure of the partial density of states around the emitting atom. In this case, the Al $L_{2,3}$ spectra were measured giving the density of s and d states around the aluminium atoms, and the Li Kβ spectra which give the partial density of p states around the lithium atoms.

The instrument used was a grazing-incidence grating spectrometer with a Bausch and Lomb blazed replica grating, platinum coated and with 1200 lines mm^{-1}. The resolution was better than 0.2 eV over the energy regions studied. A Moiré fringe angular measuring system and associated control electronics allowed repetitive scanning of the spectra without loss of resolution [3]. Each scan took approximately 35 min to complete and the sample was scraped clean between scans to avoid the build up of oxide or contaminants and to reduce modification of the surface due to the electron beam excitation source. That the scraping is effective is demonstrated by the absence of the characteristic peaks from alumina at approximately 64.7 and 68.1 eV [4] in the Al $L_{2,3}$ spectra of figure 3. Input power was kept to 3 mA at 3 kV. The operational pressure was less than 10^{-4} Pa throughout the period of measurement.

DTA was used to indicate the phase development by aging and Vickers hardness measurements were used to check the mechanical properties and to verify the DTA results. The hardness measurements also ensured that no significant room temperature aging took place over the period of the measurements. The DTA equipment had a sensitivity of 0.005 °C and an accuracy of ±2 °C. The heating rate was 10 deg min^{-1}.

The samples were cut from the commercial alloy to a size slightly greater than that required for the spectrometer. They were then solution treated at 550 °C for 1 h in air and quenched in water at room temperature. Subsequent aging at elevated temperatures was carried out also in air and the samples quenched in water. The samples were then ground down to size, which removed any surface degraded layer due to the above treatments.

To develop the most characteristic phases the following seven aging treatments were given to the alloy samples.

(1) As quenched.
(2) Aged for six days at 10^{-4} Pa at approximately 23 °C.
(3) Aged for 70 min at 140 °C.
(4) Aged for 10 h at 140 °C.
(5) Aged for 15 min at 185 °C.
(6) Aged for 15 min at 240 °C.
(7) Aged for 15 min at 280 °C.

The Al $L_{2,3}$ spectra were processed by subtracting the background intensity and normalizing the area to that of the pure metal spectrum taking account of the difference in electron-to-atom ratios. The background was extrapolated by fitting a polynomial curve to the points beyond the high and low extremities of the spectrum.

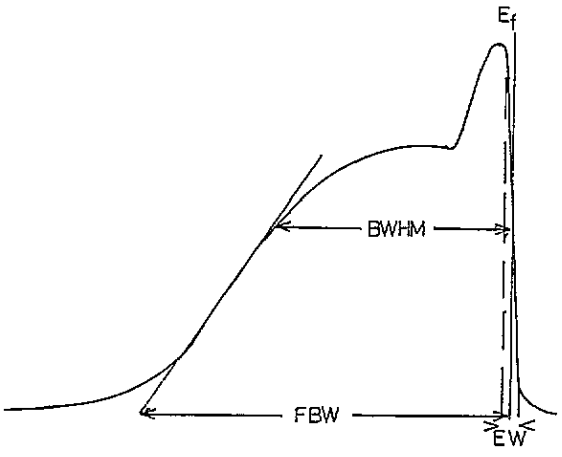

Figure 1. Schematic of an Al $L_{2,3}$ spectrum showing the derivation of the parameters.

A number of parameters have been used to highlight changes in the Al $L_{2,3}$ spectra; these, and their derivations are as follows (see figure 1).

(1) The Fermi edge, estimated by drawing a straight line through the linear portion of the emission edge and taking the energy of the mid-point between the maximum intensity and the extrapolated background.

(2) The edge width is the difference in energy between the point at which the line drawn through the emission edge crosses the extrapolated background and the point in intensity where it deviates from linearity.

(3) The band width at half maximum is measured from the Fermi edge to the low-energy limit of the band at half-maximum intensity.

(4) The full band width is the energy from the Fermi edge to the low-energy limit of the band obtained by a linear extrapolation of the low-energy tail.

(5) The average energy of the band was obtained by computer from the background subtracted spectrum from

$$\frac{\Sigma EN(E)}{\Sigma N(E)}$$

where $N(E)$ is the intensity at energy E and the summation is over the energies of the whole band.

XPS was used to measure the binding energies of the Al 2p inner core level to ensure that changes in the above parameters were not due to chemical shifts of the final state.

3. Results

At the solution treatment temperature of 550 °C, all Li, Cu and Mg is taken into solid solution. The solubility of these elements at room temperature is low and rapid cooling

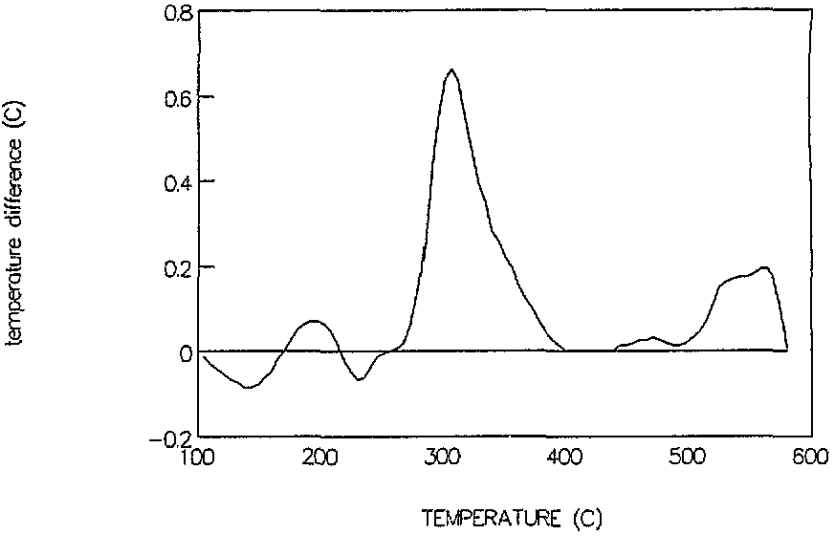

Figure 2. DTA measurement from the solution treated and quenched alloy.

produces a supersaturated solid solution (SSSS). The decomposition of this (SSSS) produces exo- and endothermic peaks on the DTA graph. Figure 2 shows the DTA scan of this alloy starting from a solution treated and quenched condition.

The DTA curve shows an initial endothermic reaction which peaks at around 140 °C. This we assign to the dissolution of GP zones formed at lower temperatures. A differential scanning calorimetric study of the same alloy by Badia *et al* [5] showed an exothermic peak in the same temperature range which became endothermic on aging at room temperature, and was accompanied by a decrease in conductivity. They explained this behaviour as being due to the formation of GP zones even though no GP zones have been observed in TEM studies. Although the presence of magnesium in Al–Li–Cu alloys has been reported to suppress the formation of Θ' in samples aged to peak hardness [6], it is possible that it will form in the early stages of aging. The most likely precipitates are copper- and lithium-based and are easily redissolved at higher temperatures during the formation of the more stable δ' and S.

The curve then becomes exothermic, peaking at around 200 °C. In this region, a number of processes could be taking place, among them the dissolution of Θ', the coarsening of δ' and the formation of S'. The DTA curve then changes slope and becomes endothermic between around 210 and 250 °C. Since δ' is reported as being stable up to 315 °C [7], it is likely that in this region, there is competition between the endothermic dissolution of Θ' and the exothermic development of S' and T_2 with the latter two predominating as temperature increases. The large exothermic peak above 300 °C is associated with precipitate coarsening and the development of equilibrium phases. The α solvus occurs at above 500 °C (T_2 is reported to exist at 520 °C [8]) and above this temperature, the single-phase solid solution is the equilibrium phase so that the exothermic regions at higher temperatures are due to the dissolution of the precipitates formed earlier.

Figures 3(a) and (b) show examples of Al $L_{2,3}$ spectra from alloys which have undergone different heat treatments superimposed on the pure aluminium spectrum. The spectra are chosen to demonstrate the distinct differences that occur due to different metastable states. A visual inspection of figures 3(a) and (b) show that structural changes occur in the spectra,

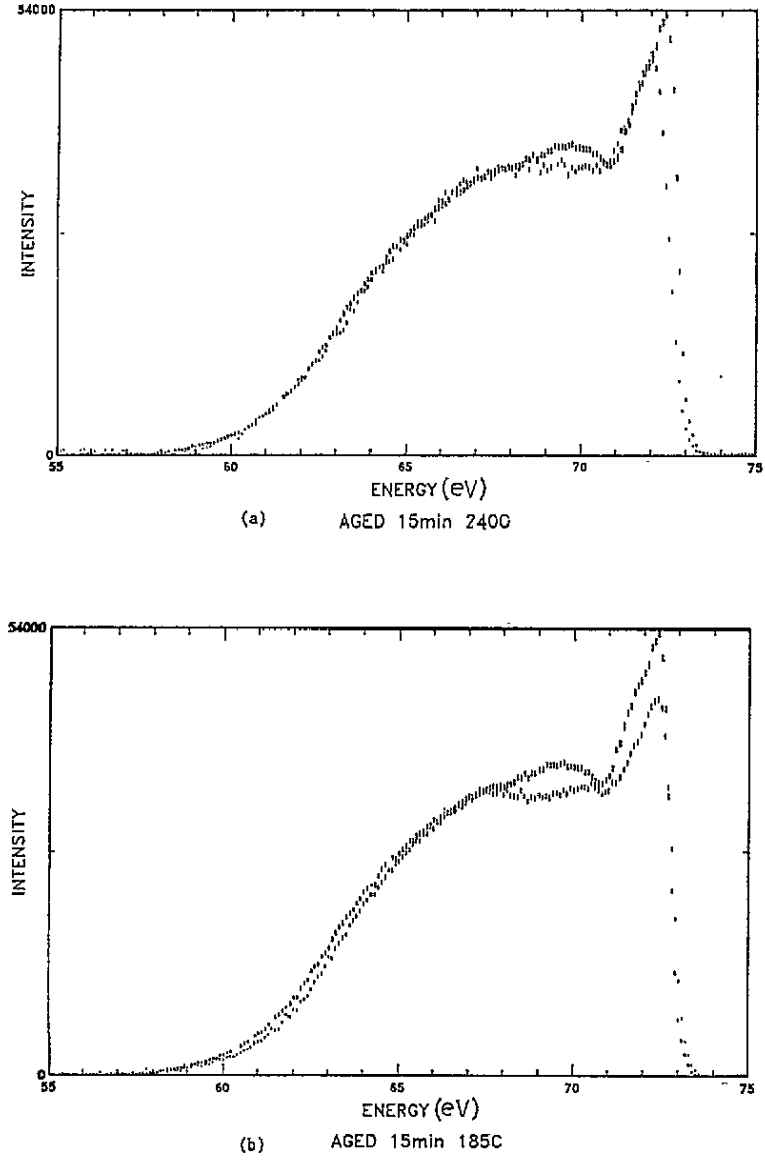

Figure 3. Al $L_{2,3}$ spectra from the alloy superimposed on the pure metal spectrum. (a) Alloy solution treated and aged for 15 min at 240 °C; (b) solution treated and aged for 15 min at 185 °C.

particularly the energy region between 67 and 71 eV. Table 2 summarizes the important parameters from these spectra.

In relation to aluminium, the position of the Fermi edge is identical for the solution-treated sample. Most other samples show a shift to lower energies. The exceptions are the sample aged at room temperature and the sample aged at 185 °C, both of which show small shifts to higher energies. All samples give an edge width greater than that recorded for pure aluminium, however, there is a large variation in this value. The sample aged for 10 h at 140 °C gives an edge width of 0.38 eV while the sample aged for 15 min at 240 °C has an

Table 2.

Sample	Edge position (eV) ±0.02	Edge width (eV) ±0.02	BWHM (eV) ±0.05	FBW (eV) ±0.1	Average energy (eV) ±0.01
1. Quenched 550 °C	72.76	0.50	7.9	12.6	68.09
2. Aged 6 d RT	72.80	0.52	7.5	12.4	68.09
3. Aged 70 min 140 °C	72.63	0.40	8.2	12.2	67.94
4. Aged 10 h 140 °C	72.62	0.38	8.0	12.2	67.85
5. Aged 15 min 185 °C	72.85	0.48	8.3	12.2	68.10
6. Aged 15 min 240 °C	72.53	0.62	7.9	12.4	67.93
7. Aged 15 min 280 °C	72.67	0.44	8.2	12.4	68.03

edge width of 0.62 eV.

The band width at half maximum is the same or larger for most samples with the maximum occurring for the sample aged at 185 °C. The exception is the sample aged for six days at room temperature which gives a BWHM value considerably smaller than that of pure aluminium. The full band widths of the alloys are the same or slightly larger than that of the pure metal. The largest value recorded was for the solution-treated sample at 12.6 eV. All other alloy samples gave values of 12.2 or 12.4 eV which compares to the pure metal value of 12.23 eV.

All alloy samples gave a lower value for the average energy of the band. The solution-treated sample, the sample aged for six days at room temperature and the sample aged for 15 min at 185 °C showed minimal decreases of 0.1 to 0.2 eV. The other samples showed more substantial decreases in keeping with the lower values returned for the Fermi edge. The relevant core levels were checked by XPS and no significant shifts were detected. Thus the decreases in average energy can be assigned to shifts in the valence band.

Figures 4(a) and (b) show the spectral region between 37 and 57 eV recorded for the same specimens with the spectrum from the as-quenched SSSS for comparison. The Li K valence band emission from the pure metal occurs between 52 and 55 eV [9] and a feature is present in all the alloy spectra in this region. The Al L_1–$L_{2,3}$ transition gives a line between 44 and 46 eV. The feature at 49.4 eV is associated with the Li K band and is due to the mixing of the lithium and aluminium valence states. This will be discussed in more detail later.

Because of the low concentration, the lithium intensity is low and superimposed on a large background intensity. The low count rate results in greater statistical variation than for the Al spectra. However, the transition rate for the Al L_1–$L_{2,3}$ line in the alloy spectra should be approximately constant and can be used as a reference to compare the intensities of other features. Hence, the intensities in figures 4(a) and (b) have been adjusted to give approximately the same height of the Al L_1–$L_{2,3}$ line. Table 3 gives the normalized peak intensities, i.e. the heights of the peaks above the background intensity in counts per second divided by the intensity of the Al L_1–$L_{2,3}$ line, and the hardness in kg mm^{-2} after the relevant heat treatment.

For the hardness values in table 3, two samples were given the same heat treatment, one for the SXS measurement and one for hardness measurements. No change in hardness occurred over the period of the SXS measurements with the exception of the sample aged for six days, which softened slightly over the aging period.

From the hardness figures of table 3 and the analysis of the DTA results given above, we infer that the most probable phases present in the alloys studied are the following. Samples 1 and 2 are most likely to be random substitutional solid solutions, perhaps with some

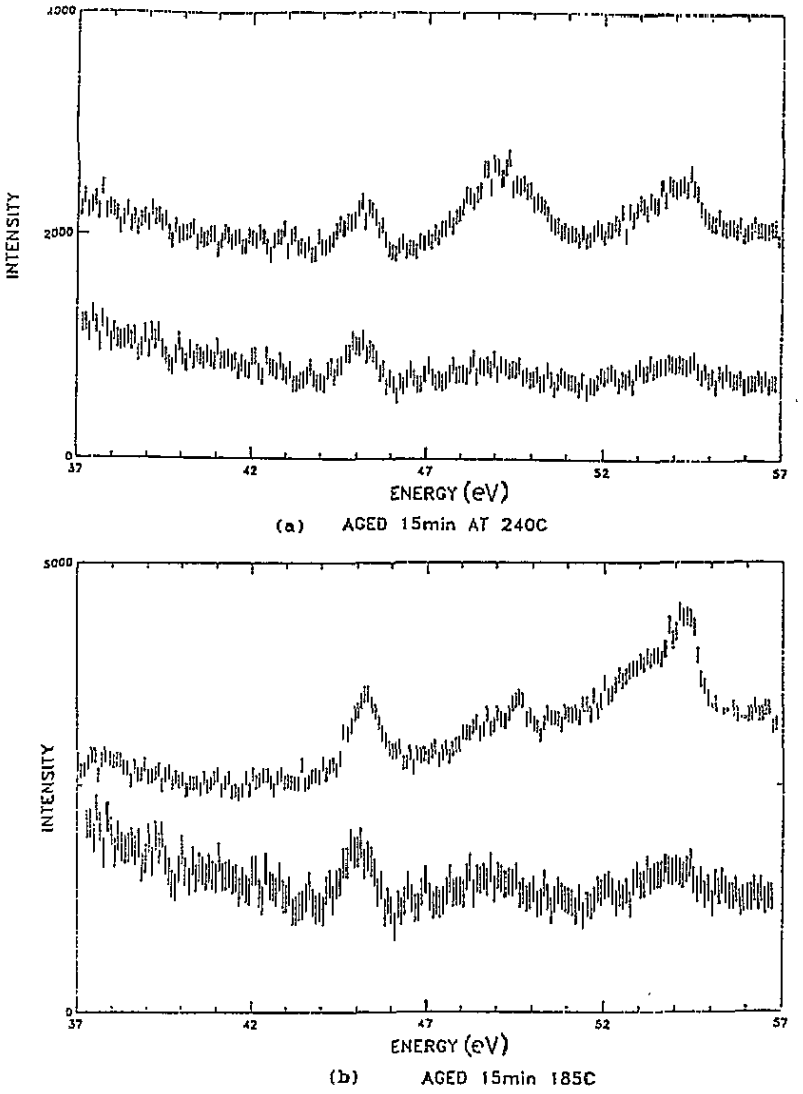

Figure 4. Li Kβ spectra from the aged alloys superimposed on that from the solution treated and quenched alloy scaled to give similar heights of the Al L_1–$L_{2,3}$ line at 45 eV. (a) Aged for 15 min at 240 °C; (b) aged for 15 min at 185 °C.

clustering, although sample 2 aged for six days at room temperature shows no increase in hardness. Samples 3 and 4, aged at 140 °C for 70 min and 10 h respectively, are hardened mainly with GP zones and the start of precipitation of δ'. Sample 5, aged at 185 °C for 15 min, has softened due to coarsening of δ' and the dissolution of Θ'. Sample 6, aged at 240 °C for 15 min, is again hardened probably due to the development of S'. The main Li bearing precipitate is still δ'. Sample 7, aged at 280 °C for 15 min, has again softened probably due to the onset of T_2 which will absorb the Li from δ'. T_2 is reported as having little hardening effect on the alloy [10].

Table 3.

Sample	$\frac{I_{54\ eV}}{I_{Al\ L_1}}$	$\frac{I_{49.4\ eV}}{I_{Al\ L_1}}$	VHN (kg mm^{-2})
1. Quenched 550 °C	0.417	0.417	85.5
2. Aged 6 d RT	0.785	0.858	80.2
3. Aged 70 min 140 °C	1.066	0.622	110.0
4. Aged 10 h 140 °C	0.668	0.266	128.0
5. Aged 15 min 185 °C	1.358	0.446	85.7
6. Aged 15 min 240 °C	1.000	1.402	118.0
7. Aged 15 min 280 °C	1.228	0.485	79.3

4. Discussion

The Al $L_{2,3}$ emission spectra represent the density of s and d states in the aluminium matrix. For aluminium and its dilute alloys, the spectra can be discussed within the framework of the nearly-free-electron model (NFE) [11]. With this assumption a free-electron parabola can be fitted to the low-energy region of the emission band after suitable allowance has been made for the many-body effects. Deviations from the free-electron parabola near the Fermi edge are attributed to changes in symmetry due to the filling of the second and third Brillouin zones. This simple picture can be complicated in alloys by the effects of hybridization and bonding but these can be expected to be small in the alloy studied here because of the dilute concentrations of the solutes. If we also assume that the partial density of p states in the valence band does not counterbalance any energy change, then the energy of the mass centre of the Al $L_{2,3}$ emission bands can be taken as a measure of the electronic contribution to the free energy of the system [12].

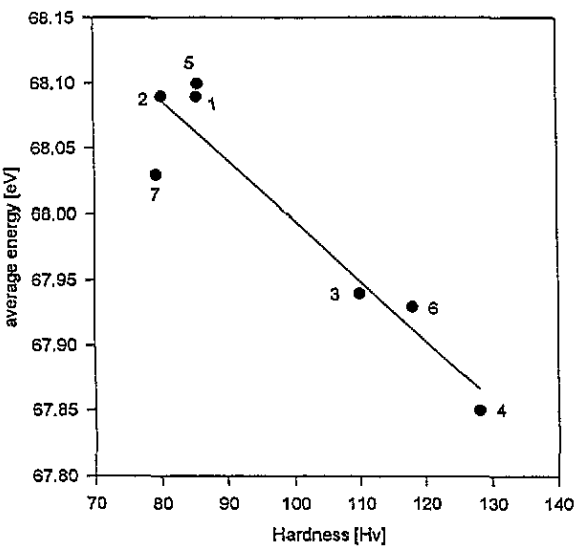

Figure 5. Average energy of the Al $L_{2,3}$ band versus hardness for the different aging treatments.

Figure 5 is a graph of the average energy of the Al $L_{2,3}$ valence band against hardness value. A straight line is a reasonable fit to the points but, more significantly, the points form two clusters. Samples 1, 2, 5 and 7 form one cluster and all showed low hardness values, while samples 3, 4 and 6 form another cluster and all had high hardness values.

Hence, samples with high hardness all showed the greatest shift to lower energies of the average energy of the Al $L_{2,3}$ valence band. Thus, it would appear that the coherent and semi-coherent precipitates which give rise to the greatest strain in the lattice and hence to the greatest hardness, is associated with a reduction in the average energy of the valence electrons. This reduction in energy gives rise to the local minimum in the free energy which is responsible for the metastability of the precipitates as postulated by Szasz *et al* [13].

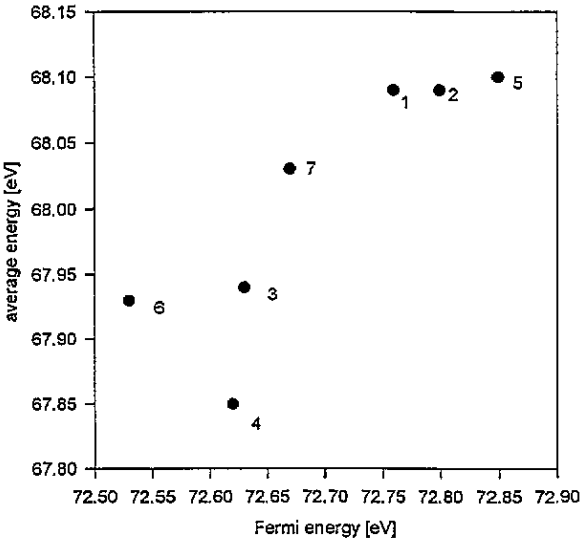

Figure 6. Average energy of the Al $L_{2,3}$ band versus Fermi energy for the different aging treatments.

Figure 6 is a plot of the average energy of the Al $L_{2,3}$ valence band versus the Fermi edge position. Most points lie on a curve, which demonstrates that changes in the average energy are due to changes in band width and not to a shift of a rigid valence band.

Little information can be derived from the Al $L_{2,3}$ spectra concerning the bonding of the aluminium in the precipitates since the majority of the signal comes from aluminium in the α matrix. However, this is not true for the lithium where most of the atoms are concentrated in the precipitates where these are formed. As shown in figures 4(a) and (b), changes to the Li K spectra with heat treatment are quite dramatic, which is not surprising since almost all the lithium in the alloy can be in a dilute solid solution or in precipitates of lithium concentration varying from 25% to approaching 50% depending on the aging treatment. For comparison, a spectrum of pure lithium, measured by Crisp and Williams [9] is shown in figure 7. The single asymmetric band has a band width of a 2.8 eV and a maximum at 54 eV. This corresponds well with the peak at 54 eV in the alloy spectra depicting a peak in the density of p states at this energy in both the pure metal and the alloy. However, the alloy spectra show an additional maximum at $\sim$ 49 eV in all the samples, and the intensity of the emission with respect to the Al L_1–$L_{2,3}$ line, and the ratio of the peak intensities both vary with heat treatment (see table 3 and figure 4).

An indication of the origin of the two alloy peaks is obtained from a theoretical calculation for a 50 at%.Al–50 at%.Li alloy using a first-principles LCAO method [14]. The partial and total density of states curves are shown in figure 8. The lithium p states show three prominent peaks occurring at -0.51, -0.67 and -0.83 Ry in the figure. Also, the density of states shows a gradual decline from the high-energy peak to almost zero at the Fermi level. A striking feature of the calculated density of states is the large p-component

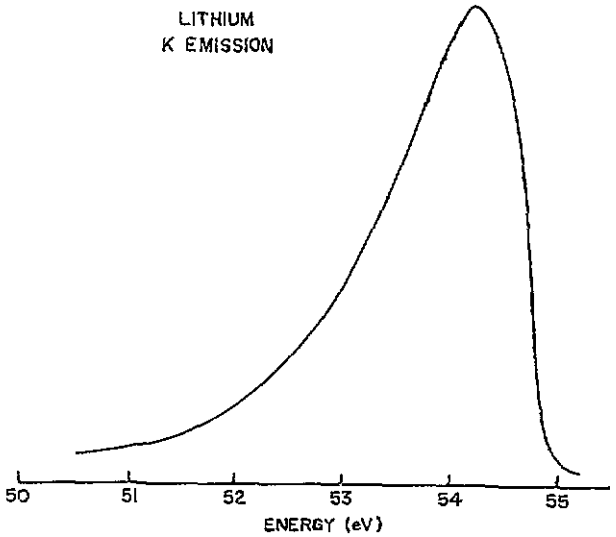

Figure 7. Li Kβ spectrum from pure lithium. From Crisp and Williams [8].

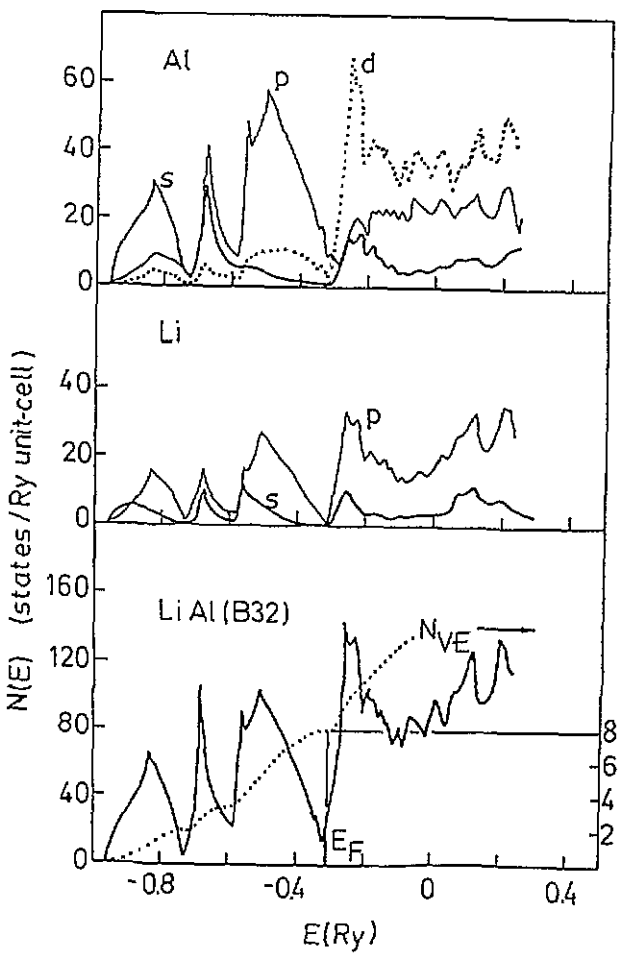

Figure 8. Calculated density of states for Al–Li. From Hafner and Weber [13].

on the aluminium sites as well as on the lithium sites. The large s to p promotion suggests sp^3 hybridization of the bonding states as found in tetrahedrally coordinated semiconductors. Comparison with the spectra aged at high temperatures where the lithium is in the δ' or T_2 precipitates does not show the gradual decline nor the three-peaked structure. However, the peaks at −0.51 Ry and −0.83 Ry in the theoretical density of states do coincide approximately with the peaks at 54 eV and 49.9 eV in the spectra. The high-energy peak corresponds to the peak in the pure metal spectrum. The low-energy peak, well below the pure metal band limit, can be attributed to s-p hybridization in the Al–Li bonds.

Table 3 shows an increase in Li K emission intensity from lithium concentrated in the precipitates over the intensity from the random solid solution suggesting an increase in the density of p states on the lithium sites due to the ordered structures.

Careful inspection of the Al $L_{2,3}$ spectra shows some structure in the region 5 to 7 eV below the Fermi edge where the calculated density of states suggests an enhancement of s-state density on the aluminium sites, particularly in the sample aged for 15 min at 185 °C. But in general, the contribution to the spectrum from the aluminium bonded to lithium in the precipitates is swamped by the emission from aluminiium in the matrix.

5. Conclusions

The production of metastable coherent and semicoherent precipitates by decomposition of a supersaturated solid solution due to suitable aging treatments is accompanied by a lowering of the average energy of the valence electrons in the alloy. The extent of the lowering is related to the hardness of the alloy and thus to the magnitude of the strain fields producing the pinning of dislocations. It is this lowering of electronic energy that is responsible for the local minimum in the free energy and hence the metastability.

In the cases where the majority of the lithium is concentrated in precipitates, the lowering of the average energy, shifts in the Fermi level and the changes in the BWHM suggest that the Al $L_{2,3}$ spectrum is not simply a superimposition of a spectrum from aluminium in the precipitates, and a spectrum from aluminium in a very dilute lithium solid solution α matrix, since the latter would dominate and not be expected to change, but rather reflects a state of the system as a whole.

Comparison of the Li K emission from the alloys with a theoretical density of states calculation for a 50/50at.% Al/Li alloy suggests that the varius ordered precipitates are striving to achieve stability by covalent-type bonding (the equilibrium phase in the binary alloy is the 50/50at.% alloy which is a Zintl compound of two interpenetrating diamond sublattices [15]).

Acknowledgments

We acknowledge with thanks a research studentship from the SERC to A Kerr in support of this work.

References

[1] Cohen J B 1986 *Solid State Phys.* **39** 131

[2] Sanders T H Jr and Starke E A Jr 1990 *Proc. Int. Conf. on Light Metals* ed T Khan and G Effenberg (Amsterdam: ASM International) p 13

[3] Watson L M, Dimond R K and Fabian D J 1967 *J. Sci. Instrum.* **44** 506
[4] Szasz A and Kojnok J 1985 *Appl. Surf. Sci.* **24** 34
[5] Badia J M, Servent R and Antoranz J M 1990 *Proc. Int. Conf. on Light Metals* ed T Khan and G Effenberg (Amsterdam: ASM International) p 81
[6] Crooks R E and Starke E A Jr 1984 *Metall. Trans.* A **15** 1367
[7] Li Y, Jones H and Warrington D H 1990 *Proc. Int. Conf. on Light Metals* ed T Khan and G Effenberg (Amsterdam: ASM International) p 65
[8] Cassada W A, Shiflet G J and Starke E A Jr 1986 *Aluminium Alloys, their Physical and Mechanical Properties* vol II, ed E A Starke Jr and T H Saunders Jr (EMAS) p 695
[9] Crisp R S and Williams S E 1960 *Phil. Mag.* **5** 1205
[10] Kim D H and Cantor B 1988 *J. Mater. Sci.* **23** 1695
[11] Rooke G A 1968 *J. Phys. C: Solid State Phys.* **1** 767
[12] Negm N Z, Watson L M and Szasz A 1987 *J. Physique* **48** C9-1033
[13] Szasz A, Kertesz L, Hajdu J and Kollar J 1985 *Aluminium* **61** 515
[14] Hafner J and Weber W 1986 *Phys. Rev.* B **33** 747
[15] McNeil M B, Pearson W B, Bennett L H and Watson R E 1973 *J. Phys. C: Solid State Phys.* **6** 1